LAWRENCE
LIVERMORE
NATIONAL
LABORATORY

LLNL-JRNL-408883

Water confined in carbon nanotubes: Magnetic response and proton chemical shieldings

P. Huang, E. Schwegler, G. Galli

November 19, 2008

Journal of Physical Chemistry C

Disclaimer

Water confined in carbon nanotubes: Magnetic response and proton chemical shieldings

Patrick Huang,[†] Eric Schwegler,[*,†] and Giulia Galli[‡]

Physics and Life Sciences Directorate, Lawrence Livermore National Laboratory, 7000 East Ave., Livermore, CA 94551, and Department of Chemistry, University of California, One Shields Ave., Davis, CA 95616

E-mail: schwegler@llnl.gov

November 12, 2008

Abstract

We study the proton nuclear magnetic resonance (^{1}H-NMR) of a model system consisting of liquid water in infinite carbon nanotubes (CNT). Chemical shieldings are evaluated from linear response theory, where the electronic structure is derived from density functional theory (DFT) with plane-wave basis sets and periodic boundary conditions. The shieldings are sampled from trajectories generated via first-principles molecular dynamics simulations at ambient conditions, for water confined in (14,0) and (19,0) CNTs with diameters $d = 11$ Å and 14.9 Å, respectively. We find that confinement within the CNT leads to a large (~ -23 ppm) *upfield* shift relative to bulk liquid water. This shift is a consequence of strongly anisotropic magnetic fields induced in the CNT by an applied magnetic field.

[†]Lawrence Livermore National Laboratory
[‡]University of California, Davis

The complex behavior of water in nanoscale cavities, channels, and interfaces is fundamental to a broad range of phenomena, and can be quite different from bulk phases. In particular, single-walled carbon nanotubes (CNT) provide a well-defined environment to study confinement effects,[1] and serve as a model for more complicated systems, *e.g.*, biological membrane channels. Novel nanoscale properties of water confined to CNT channels include the experimental observation of fast water transport[2] and ion exclusion,[3] demonstrating the potential of CNT-based materials for advanced nanofluidic applications.

Simulations have been crucial in elucidating the microscopic origins of such unusual phenomena. However, simulations are subject to a certain number of assumptions; in particular, approximations are made in the modeling of interatomic forces. Most theoretical work on confined water so far have relied on semiempirical model potentials that are typically fit to reproduce known bulk behavior, whose applicability to confined water may be questionable. Strategies where interatomic forces are evaluated from first principles electronic structure methods can provide a more unbiased picture, without input from experiment. At present, such calculations are expensive, and limited to water confined to narrow ($d < 1.5$ nm) CNTs for short (≤ 20 ps) time scales.[4] Therefore, progress requires exchange between theory and experiment, and it is essential to relate theoretical models to experimentally accessible observables that can be tested and validated in the laboratory.

One important class of observables is nuclear magnetic resonance (NMR), whose use in the structural studies of molecules and proteins is well-established. NMR techniques can resolve the different resonance frequencies of non-equivalent nuclei, thus providing a detailed, atomic-scale probe of the local electronic structure. The relaxation of nuclear spins contains information about rotational and diffusional correlation times, and is sensitive to local ordering (*i.e.*, solid versus liquid). This feature has been exploited to track the onset of freezing in CNT-confined water.[5–7] Unfortunately, it is difficult to prepare clean, uniform CNT samples for high resolution measurements. Usually, CNT samples contain a mixture of semiconducting and metallic nanotubes with different diameters and chiralities. Defects can be present at non-negligible concentrations, depending on the preparation conditions. In addition, CNTs are often contaminated with the transition metal

catalysts employed in their synthesis, and the presence of such paramagnetic impurity centers lead to large inhomogeneous broadenings in NMR spectra.

It is therefore not surprising that there are significant discrepancies among NMR studies of water in CNTs. The ^{1}H-NMR chemical shift associated with confined water in CNTs has been reported at values ranging from around $+8$ ppm downfield to -15 ppm upfield relative to the bulk water proton resonance.[5–8] Given the uncertainty in the experiments, it is important to establish a theoretical baseline value for the ^{1}H-NMR signature of confined water in an ideal, model system. To this end, we evaluate the ^{1}H-NMR chemical shielding tensors for water in infinite, defect-free CNTs. These shieldings are compared to the proton shieldings for bulk water under standard conditions, which is an important test case of our methodology, and serves as a point of reference for the study of confinement effects. Our results indicate that the interior of the CNTs induces a significant upfield shift for confined water as compared to bulk liquid water, in qualitative agreement with the most recent experiments.

Theory and computational details. The application of a uniform magnetic field $\mathbf{B}_0$ to atoms and molecules induces an inhomogeneous electron current density $\mathbf{J}_{\rm ind}(\mathbf{r})$. From classical magnetostatics, the induced field $\mathbf{B}_{\rm ind}(\mathbf{r})$ generated by this current is given by the Biot-Savart law:

$$\mathbf{B}_{\rm ind}(\mathbf{r}) = \frac{1}{c}\int d\mathbf{r}'\, \mathbf{J}_{\rm ind}(\mathbf{r}') \times \frac{\mathbf{r}'-\mathbf{r}}{|\mathbf{r}'-\mathbf{r}|^3}. \tag{1}$$

We consider the linear response to the external field, so that the induced field can be expressed as

$$\mathbf{B}_{\rm ind}(\mathbf{r}) = -\boldsymbol{\sigma}(\mathbf{r})\cdot\mathbf{B}_0. \tag{2}$$

The tensor $\boldsymbol{\sigma}(\mathbf{r})$ characterizes the shielding of $\mathbf{B}_0$ by the electrons, and reflects the details of the local electronic structure. NMR probes $\boldsymbol{\sigma}(\mathbf{r})$ at nuclear positions $\mathbf{r} = \mathbf{r}_{\rm X}$; in this case, it is referred to as the chemical shielding tensor associated with nuclei X.

For periodic systems, $\mathbf{J}_{\rm ind}(\mathbf{r})$, $\mathbf{B}_{\rm ind}(\mathbf{r})$, and $\boldsymbol{\sigma}(\mathbf{r})$ are periodic functions of $\mathbf{r}$, and so it is more convenient to work in their Fourier representations. The $\mathbf{G} \neq 0$ Fourier components of $\mathbf{B}_{\rm ind}(\mathbf{r})$ are

evaluated from Eq. (1) as

$$\widetilde{\mathbf{B}}_{\mathrm{ind}}(\mathbf{G}\neq 0) = i\frac{4\pi}{c}\frac{\mathbf{G}}{|\mathbf{G}|^2}\times\widetilde{\mathbf{J}}_{\mathrm{ind}}(\mathbf{G}), \tag{3}$$

and substituting into the Fourier transform of Eq. (2) gives the $\mathbf{G}\neq 0$ components of the shielding tensor. The $\mathbf{G}=0$ component is handled separately, for the evaluation of $\widetilde{\mathbf{B}}_{\mathrm{ind}}(\mathbf{G}=0)$ involves an integration of $\mathbf{B}_{\mathrm{ind}}(\mathbf{r})$ over the entire volume of the macroscopic sample, which requires the specification of its shape. A common choice is a spherical sample, so that

$$\widetilde{\mathbf{B}}_{\mathrm{ind}}(\mathbf{G}=0) = 4\pi\alpha\chi_v\cdot\mathbf{B}_0, \tag{4}$$

where α is a diagonal tensor with $\alpha_{xx}=\alpha_{yy}=\alpha_{zz}=2/3$, and χ_v is the magnetic volume susceptibility tensor.[9] For a cylindrical sample with the cylinder axis along the z-direction, $\alpha_{xx}=\alpha_{yy}=1/2$ and $\alpha_{zz}=1$. The $\mathbf{G}=0$ Fourier component of $\boldsymbol{\sigma}(\mathbf{r})$ is thus

$$\widetilde{\boldsymbol{\sigma}}(\mathbf{G}=0) = -4\pi\alpha\chi_v. \tag{5}$$

While the accurate quantum chemical evaluation of chemical shielding tensors of small molecules has been routine for several decades, only within this last decade have methods emerged that can treat the magnetic response of extended systems under 3D periodic boundary conditions. Here, we evaluate $\boldsymbol{\sigma}(\mathbf{r})$ in the above periodic formulation, using the gauge-included projector augmented wave (GIPAW) method[10] as implemented in the QUANTUM-ESPRESSO[11] suite of plane-wave electronic structure codes. The GIPAW method is based on earlier work by Mauri *et al.* on the evaluation of the magnetic susceptibility χ_v and chemical shielding tensor $\boldsymbol{\sigma}(\mathbf{r})$ within the pseudopotential approximation.[9,12] GIPAW goes beyond pseudopotentials to obtain $\boldsymbol{\sigma}(\mathbf{r})$ with an all-electron, frozen core treatment.

In short, the GIPAW procedure begins with the zeroth-order electronic wavefunctions $\{\psi_n^{(0)}\}$ in the absence of $\mathbf{B}_0$. In the present case, we use Kohn-Sham density functional theory (DFT) with the PBE approximation[13] for exchange-correlation, using a plane-wave basis set truncated at

$E_c = 70$ Ry. For the systems of interest here, increasing this cutoff to $E_c = 85$ Ry only changes the shieldings by ~ 0.01 ppm. The first-order wavefunctions $\{\psi_n^{(1)}\}$ are then evaluated from the linear response to the perturbation due to the presence of $\mathbf{B}_0$, from which the induced current $\mathbf{J}_{\text{ind}}(\mathbf{r})$ is obtained. Finally, the induced field $\mathbf{B}_{\text{ind}}(\mathbf{r})$ and shielding tensor $\boldsymbol{\sigma}(\mathbf{r})$ are computed according to Eqs. (1)–(4).

Since the focus of this work is on ^{1}H-NMR chemical shieldings, from this point on $\boldsymbol{\sigma} = \boldsymbol{\sigma}(\mathbf{r}_{\text{H}})$ unless otherwise noted. In a liquid, molecules are tumbling rapidly relative to typical NMR timescales ($\sim 10^{-6}$ s) and so one effectively measures an orientationally-averaged, isotropic shielding,

$$\sigma_{\text{iso}} = \frac{1}{3}\text{Tr}[\boldsymbol{\sigma}]. \tag{6}$$

The most immediate quantity from NMR is the chemical shift δ, which is a difference in isotropic shieldings,

$$\delta = \sigma_{\text{iso}}^{\text{ref}} - \sigma_{\text{iso}}, \tag{7}$$

where $\sigma_{\text{iso}}^{\text{ref}}$ is the shielding at nuclei X in some reference compound, and σ_{iso} is the shielding of the same nuclei X in the compound of interest. A positive (downfield) shift means the nuclei of interest is *less* shielded than the reference, while a negative (upfield) shift means the nuclei of interest is *more* shielded than the reference. The chemical shielding anisotropy $\Delta\sigma$ is defined as

$$\Delta\sigma = \sigma_{11} - \frac{1}{2}\left(\sigma_{22} + \sigma_{33}\right), \tag{8}$$

where $\sigma_{11}, \sigma_{22}, \sigma_{33}$ are the principal values of the irreducible rank 1 tensor $\boldsymbol{\sigma}^{(1)} = \left(\boldsymbol{\sigma} + \boldsymbol{\sigma}^T\right)/2$, with $\sigma_{11} > \sigma_{22} > \sigma_{33}$.

Bulk liquid water. We consider bulk liquid water at ambient conditions as the reference state, and compute ^{1}H chemical shieldings with a spherical susceptibility correction $\alpha = 2/3$ [Eq. (4)]. The thermally-averaged isotropic shielding $\langle\sigma_{\text{iso}}^{\text{liq}}\rangle$ is evaluated by averaging σ_{iso} of each water molecule over configurations from first-principles molecular dynamics (FPMD). We sample $N_c = 15$ configurations from an FPMD trajectory generated with classical Born-Oppenheimer dynamics,

for $N = 64$ water molecules in a cubic box of size $a = 12.43$ Å. A simulation temperature of $T = 400$ K was used to partly mimic proton quantum effects at $T = 300$ K. Such a temperature rescaling was previously shown to yield radial distribution functions that are in good agreement with experiment at $T = 300$ K.[14,15] Statistical errors are estimated by averaging σ_{iso} of all protons in an individual FPMD configuration, and taking the population standard deviation of the set of configuration averages.

Our results are summarized in Table 1, and compared to previous theoretical bulk water studies under periodic boundary conditions, and experiment. Among the prior theoretical studies, the most direct comparison with ours is the work of Pfrommer *et al.*,[16] who use a DFT-based linear response approach similar to that employed here. However, there are differences in the underlying details, the most significant being the FPMD simulations used to generate the water configurations. Ref. 16 averages over $N_c = 9$ configurations sampled from the Car-Parrinello simulation of Sprik *et al.*,[17] which was performed for a smaller box of $N = 32$ water molecules at $T = 300$ K. There, a rather large value of $\mu = 1100$ a.u. was chosen for the fictitious electron mass that is needed in the Car-Parrinello scheme. Despite these differences, our result for $\langle\sigma_{\mathrm{iso}}^{\mathrm{liq}}\rangle$ agrees closely with Ref. 16. While such excellent agreement may be somewhat fortuitous, it is not unreasonable as the underlying FPMD simulations in both cases give similar results for the overall liquid water structure.

Table 1: Thermally-averaged isotropic proton shielding $\langle\sigma_{\mathrm{iso}}^{\mathrm{liq}}\rangle$ and shielding anisotropy $\langle\Delta\sigma^{\mathrm{liq}}\rangle$ for bulk liquid water. Ref. 18 reports only the gas-to-liquid chemical shift $\delta = \sigma_{\mathrm{iso}}^{\mathrm{gas}} - \langle\sigma_{\mathrm{iso}}^{\mathrm{liq}}\rangle$. All shieldings are in units of ppm.

	$\langle\sigma_{\mathrm{iso}}^{\mathrm{liq}}\rangle$	δ	$\langle\Delta\sigma^{\mathrm{liq}}\rangle$
This work	24.3(3)		26.9(5)
Ref. 16	24.3(1)[a]	5.8(1)	
Ref. 18		5.2(2)	
Ref. 19 (expt.)	25.71(2)[b]		27.4(1)

[a] Converted to an absolute shielding using the reported value for the reference shielding $\sigma_{\mathrm{iso}}^{\mathrm{gas}}$. Ref. 16 evaluates the statistical error as the sample standard deviation of all proton shieldings over all configurations.

[b] Ref. 19 derives an absolute shielding using the chemical shift relative to CH_4 gas; see reference for details.

Sebastiani and Parrinello[18] also use a DFT-based linear response approach, but there the mag-

netic perturbation under periodic boundary conditions is handled differently from this work and Ref. 16. The water configurations are generated by the CPMD simulations of Silvestrelli *et al.*,[20] which should be similar ($N = 32$, $T = 303$ K, $\mu = 900$ a.u.) to that used in Ref. 16. Ref. 18 does not report averaged absolute shieldings, only the gas-to-liquid shift.

While changes in the isotropic shielding $\sigma_{\rm iso}$ are usually taken as qualitative signatures of hydrogen bonding, the shielding anisotropy $\Delta\sigma$ is a much more sensitive measure of hydrogen bond formation and geometry than $\sigma_{\rm iso}$.[21,22] For solids, high-resolution, solid-state NMR techniques can determine the orientation and principal values of the shielding tensor. These methods are not applicable to the liquid state, where information about the components of the shielding tensor is averaged out by molecular tumbling. To our knowledge, the only measurement of $\langle\Delta\sigma^{\rm liq}\rangle$ in liquid water is by Modig *et al.*, who extract $\langle\Delta\sigma^{\rm liq}\rangle$ from proton spin relaxation rates.[19] Average hydrogen bond distances and angles were subsequently inferred by fitting to a geometrical model relating the liquid structure to $\langle\sigma_{\rm iso}^{\rm liq}\rangle$ and $\langle\Delta\sigma^{\rm liq}\rangle$.[22]

Here, we evaluate $\langle\Delta\sigma^{\rm liq}\rangle$ by computing $\Delta\sigma$ for each proton from its instantaneous principal value, and then averaging the individual $\Delta\sigma$ over configurations. This averaging is done over the same $N_c = 15$ configurations used in the evaluation of $\langle\sigma_{\rm iso}^{\rm liq}\rangle$ above. The result is listed in Table 1, along with the experimental value from Ref. 19. While the ability of FPMD simulations to reproduce the correct radial structure in liquid water has been demonstrated, the good agreement seen between the theoretical and experimental value for $\langle\Delta\sigma^{\rm liq}\rangle$ confirms the ability of the FPMD to give the correct angular structure as well.

Water in carbon nanotubes. First-principles calculations for the magnetic response and ^{13}C-NMR chemical shifts of empty, infinite CNTs have been reported previously.[23–26] Here, we evaluate ^{1}H-NMR shieldings of water enclosed in semiconducting, zigzag (14,0) and (19,0) CNTs, whose diameters are $d = 11.0$ Å and $d = 14.9$ Å, respectively. In order to isolate the effects of the nanotube, we begin by considering a single water molecule in a (14,0) CNT. The water/(14,0) nanotube system is modeled in a tetragonal supercell with lattice parameters $a = b = 17.0$ Å, and $c = 12.7607$ Å, which corresponds to three primitive nanotube unit cells along the c-axis, and 6 Å

of vacuum between nanotubes. The susceptibility corrections to the chemical shieldings [Eq. (4)] are evaluated as $\alpha_{xx} = \alpha_{yy} = 1/2$ and $\alpha_{zz} = 2/3$. This choice was previously shown to yield the fastest convergence of the ^{13}C-NMR chemical shifts with respect to the inter-tube spacing,[25] which we have also verified here. Integration over the Brillouin zone is done using six k-points spaced $\Delta k = 0.04924$ Å^{-1} apart. These computational parameters are similar to those in Ref. 25 (except for the plane-wave basis cutoff E_c, which is necessarily higher here due to the presence of oxygen atoms), and yield ^{1}H-NMR shieldings that are converged to < 0.5 ppm.

The water molecule is positioned with the oxygen at the CNT center, in two different orientations: one O-H bond oriented parallel to the tube axis, and both O-H bonds perpendicular to the tube axis. Table 2 lists the principal values for the proton shieldings, along with the isolated molecule values (*i.e.*, no CNT present). Upon encapsulation in a CNT, the most dramatic change is a $\delta \sim -22$ ppm upfield shift in $\sigma_{\rm iso}$, relative to the isolated molecule. This is quite large, considering that typical proton chemical shifts in small organic molecules are $\delta \sim 0-10$ ppm downfield relative to tetramethylsilane (TMS). The change in $\sigma_{\rm iso}$ upon encapsulation is at least an order of magnitude larger than changes due to intramolecular distortions, or the relative position of the molecule within the CNT. On the other hand, $\Delta\sigma$ is sensitive to the orientation of the water relative to the tube axis. Inside the CNT, the largest decrease in $\Delta\sigma$ (~ -9 ppm) occurs when the O-H bond is parallel to the tube axis, while the largest increase (~ 12 ppm) occurs when the O-H bond is perpendicular to the tube axis.

Similar behavior is also seen in the calculations of Besley and Noble for the proton chemical shifts of a variety of small molecules in CNTs. In general, they find upfield shifts relative to the isolated molecules, on the order of around -13 ppm to -26 ppm for the zigzag CNTs.[27] However, the study of Ref. 27 differs significantly from ours. In particular, they model finite, hydrogen-capped CNTs using molecular quantum chemical methods with localized, Gaussian basis sets (gauge-including atomic orbitals method), while we consider here an infinite CNT with plane-wave basis sets. Zurek *et al.*[23] have made a direct comparison between ^{13}C-NMR shifts in capped and infinite CNTs, and found very slow convergence of the capped CNTs with respect to

Table 2: Principal values σ_{11}, σ_{22}, and σ_{33} of the proton shielding tensor, isotropic shielding $\sigma_{\rm iso}$, and shielding anisotropy $\Delta\sigma$ for the water molecule. The three sets of values correspond to: no CNT present, one O-H bond parallel to the tube axis ($H_{\parallel}$), and both O-H bonds perpendicular to the tube axis ($H_{\perp}$). All shieldings are in units of ppm.

	σ_{11}	σ_{22}	σ_{33}	$\sigma_{\rm iso}$	$\Delta\sigma$
No CNT:					
H	41.43	25.56	23.41	30.13	16.95
Parallel:					
$H_{\parallel}$	57.84	54.46	46.27	52.86	7.48
H	70.82	54.32	33.33	52.82	27.00
Perpendicular:					
$H_{\perp}$	72.62	56.45	29.43	52.83	29.68

tube length; this is consistent with our own observations of finite-size effects on ^{1}H-NMR shifts in CNTs.

We check whether this strongly diamagnetic environment is restricted to the interior of the CNT by considering water molecules outside a nanotube. In an actual sample, nanotubes typically aggregate in bundles, creating interstitial regions that molecules could potentially occupy. This is modeled as a hexagonal array of CNTs with a single water molecule in the hollow sites. The interstital water is oriented with one O-H bond parallel to the CNT, and the second O-H pointing towards the region between two adjacent CNTs. We did not attempt to optimize atom positions, as the aim here is to qualitatively probe the proton shielding in these regions. Brillouin zone sampling is done using a 4×4 *k*-point mesh along the lateral directions, and the sampling along the *c*-axis is the same as the isolated nanotube calculations above. A cylindrical susceptibility correction [Eq. (4)] of $\alpha_{xx} = \alpha_{yy} = 1/2$ and $\alpha_{zz} = 1$ is used. We find a *downfield* proton shift of $\delta \sim 1.7$ ppm and $\delta \sim 0.5$ ppm relative to the isolated water molecule, with the smaller shift due to the proton on the parallel O-H bond. While the direction of the shift is opposite to that of water inside the CNT, the magnitude is not nearly as dramatic.

It is unlikely that the large effects of the CNT on the confined water shieldings are due to chemical bonding interactions, as the water is positioned too far from the carbon atoms in the cases discussed above. Instead, these effects can be understood as originating from induced currents on the

CNT. This is analogous to the textbook example of ring currents in benzene and other π-conjugated molecules, which generate a strongly anisotropic induced field that causes large chemical shifts in nearby protons. In CNTs, the application of an external magnetic field along the tube axis generates extended currents encircling the circumference of the nanotube, whose topology creates a strongly diamagnetic environment inside the nanotube.[26] Here, we have quantified these effects on the proton isotropic shift, and demonstrated the sensitivity of the shielding tensor components to the orientation of the encapsulated water molecule.

We see similar behavior in the thermally-averaged isotropic proton shielding $\langle\sigma_{\text{iso}}^{\text{liq}}\rangle$ for liquid-filled (14,0) and (19,0) CNTs. The (14,0) CNT contains 34 water molecules in a tetragonal supercell similar to the one used for the single water molecule calculations above, except with a longer length $c = 25.52$ Å. This corresponds to six primitive nanotube unit cells along the c-axis. The averaged isotropic shielding $\langle\sigma_{\text{iso}}^{\text{liq}}\rangle$ and shielding anisotropy $\langle\Delta\sigma^{\text{liq}}\rangle$ are evaluated by sampling $N_c = 12$ configurations from the FPMD simulation of Cicero *et al.*[4] As with bulk water, the FPMD simulations were run at $T = 400$ K. The liquid-filled (19,0) CNT is modeled similarly, except it contains 54 water molecules in a supercell with length $c = 17.06$ Å, corresponding to four primitive nanotube unit cells along the c-axis.

Table 3: Thermally-averaged proton shielding $\langle\sigma_{\text{iso}}^{\text{liq}}\rangle$ and shielding anisotropy $\langle\Delta\sigma^{\text{liq}}\rangle$ for liquid water in a (14,0) and (19,0) CNT with diameter d. The shift δ is referenced relative to the computed bulk water isotropic shielding of 24.3(3) ppm (Table 1). All shieldings are in units of ppm.

	d	$\langle\sigma_{\text{iso}}^{\text{liq}}\rangle$	$\langle\Delta\sigma^{\text{liq}}\rangle$	δ
(14,0)	11.0 Å	48.5(4)	25.3(5)	−24.2(5)
(19,0)	14.9 Å	47.1(8)	25.3(7)	−22.8(9)

The results are summarized in Table 3. Like the single encapsulated molecule, the most noticeable effect in the confined liquid is the large upfield shift in $\langle\sigma_{\text{iso}}^{\text{liq}}\rangle$ relative to free bulk water. Again, the size of this shift is much larger than changes expected from reasonable variations in the liquid structure or computational parameters in the DFT linear response methodology. On the other hand, the confined liquid $\langle\Delta\sigma^{\text{liq}}\rangle$ is similar to that of free bulk water. Given the above observations for single molecules, $\langle\Delta\sigma^{\text{liq}}\rangle$ is sensitive to both hydrogen bonding in the liquid, and the orientation

of individual water molecules relative to the CNT axis. The computed shieldings for water in the (14,0) and (19,0) tubes are very similar, and more statistical sampling would be required in order to clearly resolve any differences.

Figure 1 shows the shieldings of individual protons as a function of radial distance r from the center of the (14,0) and (19,0) CNTs. The corresponding radial hydrogen density distributions from Ref. 4 are also shown. The spread in proton shieldings is generally quite large, which reflects the sensitivity of the proton shieldings to the local hydrogen bond environment. A similar effect was also seen in the bulk water studies of Refs. 18 and 22. Nevertheless, one clear feature is evident: in both the (14,0) and (19,0) CNTs, the distribution of σ_{iso} for protons closest to the CNT wall exhibits a significant narrowing and shift to higher values, while the distribution of $\Delta\sigma$ narrows and shifts to lower values.

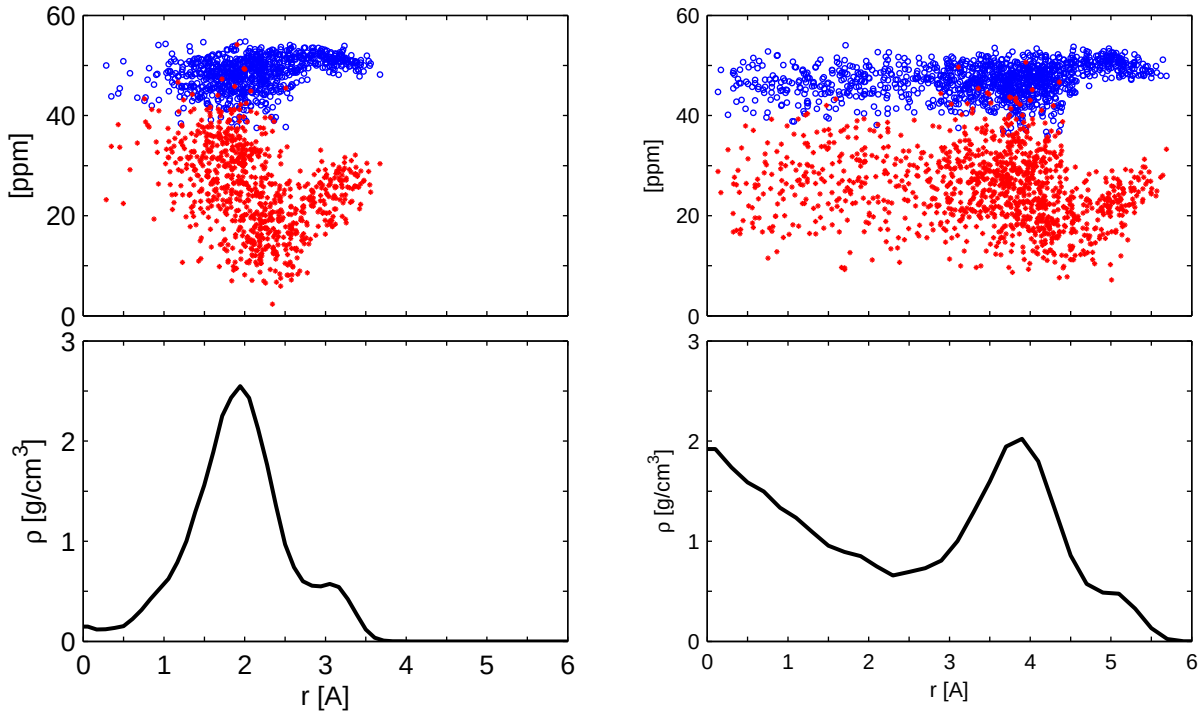

Figure 1: (color on-line) Upper panels: Isotropic shielding σ_{iso} (blue) and shielding anisotropy $\Delta\sigma$ (red) for individual water protons in a (14,0) CNT (left) and (19,0) CNT (right), as a function of distance r from the nanotube center. Lower panels: Corresponding proton densities, adapted from Ref. 4. The (14,0) CNT radius is 5.5 Å, and the (19,0) CNT radius is 7.45 Å.

As previously described in Ref. 4, the CNT-confined water has an interfacial layer that peaks at about 3.5 Å from the CNT wall. The water molecules in this interfacial layer are mostly arranged to form hydrogen bonds parallel to the CNT wall. The small shoulder seen in this first density peak is due to a slight preference for molecules to orient with a non-hydrogen-bonded O-H pointing out towards the CNT wall. By comparison with the radial densities, the qualitative changes in the shieldings at the interface correlate with these non-hydrogen-bonded O-H, which are shifted upfield relative to the other hydrogen-bonded protons. The main difference in the confined liquid structure for the (14,0) and (19,0) CNTs is that the smaller (14,0) CNT essentially contains just interfacial water with very little liquid in the center of the nanotube, while the (19,0) CNT is large enough to hold both an interfacial layer and a bulk-like fluid in the interior.

There is a large spread in the experimental values for the isotropic proton shifts of water confined in CNTs, which is likely to be due to different CNT preparation procedures, as well as the precise details of how the measurements are carried out. The early experiments of Ghosh *et al.*[5] report a confined water resonance at 13.8 ppm and free bulk water at 4.6 ppm, implying that confinement in CNTs results in a +9.2 ppm *downfield* shift relative to bulk water. Sekhaneh *et al.*[6] and Chen *et al.*[8] subsequently employed magic angle spinning techniques to improve the spectral resolution; both studies found the confined water resonance to be shifted *upfield* relative to their reported resonances for free bulk water, by -3.3 ppm[6] and -4.4 ppm,[8] respectively. Matsuda *et al.*[7] report a larger ~ -15 ppm upfield shift for the confined water relative to free bulk water.

The theoretical calculations here for the liquid-filled CNTs find large upfield shifts relative to bulk water, that are around -8 ppm to -9 ppm farther upfield than the results of Matsuda *et al.*[7] In general however, one must be careful in making a direct comparison between our ideal, defect-free, single CNT model with experiments, as the process of opening the CNTs will certainly introduce defects that can potentially obscure the experimental data. We have repeated the single encapsulated water molecule studies above, using instead a CNT with a single Stone-Wales defect,[28] but the differences were minor compared to the large proton shifts induced by the defect-free CNT. However, this may or may not be representative of the types of defects formed during sample

preparation, and a thorough survey of possible defects is beyond the scope of this work. We note that a recent experimental study using a gentler procedure to remove end caps report a ^{1}H-NMR spectra for ethane gas in CNTs. A broad resonance for confined ethane is observed, whose peak is shifted by > 50 ppm upfield relative to the free ethane resonance.[29]

In summary, we have evaluated the magnetic response and ^{1}H-NMR chemical shieldings of water confined in ideal, infinite CNTs. The calculations are done using a DFT-based linear response theory with plane-wave basis sets and periodic boundary conditions. The confined water resonance is shifted upfield relative to free, bulk water. This is consistent with previous theoretical work on empty CNTs, which find a strongly diamagnetic environment in the interior, as well as with the more recent experiments reported to date. For the liquid-filled CNT, we find the magnitude of the confined water shift to be ~ -23 ppm upfield relative to free bulk water, which is still large compared to the range of -3.3 ppm to -15 ppm seen in experiments so far. However, the large spread in the experimental values suggest that the actual shift is probably very sensitive to details involved in sample preparation. A more detailed examination of the proton shieldings for the confined liquid reveals a component associated with non-hydrogen-bonded O-H groups at the immediate interface between the liquid and the CNT wall, and a component due to the bulk-like interior. Future work will consider the role of defects on confined water chemical shifts.

Acknowledgments We thank Julie Herberg and Jason Holt for helpful discussions regarding the ^{1}H-NMR experiments. This work was partly performed under the auspices of the U.S. Department of Energy by Lawrence Livermore National Laboratory under Contract DE-AC52-07NA27344, and partly supported by the Office of Science, U.S. Department of Energy, SciDAC grant DE-FC02-06ER46262. Use of computer resources from Lawrence Livermore National Laboratory and the Innovative and Novel Computational Impact on Theory and Experiment (INCITE) program are gratefully acknowledged.

References

(1) Rasaiah, J. C.; Garde, S.; Hummer, G. *Annu. Rev. Phys. Chem.* **2008**, *59*, 713.

(2) Holt, J. K.; Park, H. G.; Wang, Y.; Stadermann, M.; Artyukhin, A. B.; Grigoropoulos, C. P.; Noy, A.; Bakajin, O. *Science* **2006**, *312*, 1034.

(3) Fornasiero, F.; Park, H. G.; Holt, J. K.; Stadermann, M.; Grigoropoulos, C. P.; Noy, A.; Bakajin, O. *Proc. Natl. Acad. Sci. U.S.A.* **2008**.

(4) Cicero, G.; Grossman, J. C.; Schwegler, E.; Gygi, F.; Galli, G. *J. Am. Chem. Soc.* **2008**, *130*, 1871.

(5) Ghosh, S.; Ramanathan, K. V.; Sood, A. K. *Europhys. Lett.* **2004**, *65*, 678.

(6) Sekhaneh, W.; Kotecha, M.; Dettlaff-Weglikowska, U.; Veeman, W. S. *Chem. Phys. Lett.* **2006**, *428*, 143.

(7) Matsuda, K.; Hibi, T.; Kadowaki, H.; Kataura, H.; Maniwa, Y. *Phys. Rev. B* **2006**, *74*, 073415.

(8) Chen, Q.; Herberg, J. L.; Mogilevsky, G.; Wang, H.-J.; Stadermann, M.; Holt, J. K.; Wu, Y. *Nano Lett.* **2008**, *8*, 1902.

(9) Mauri, F.; Louie, S. G. *Phys. Rev. Lett.* **1996**, *76*, 4246.

(10) Pickard, C. J.; Mauri, F. *Phys. Rev. B* **2001**, *63*, 245101.

(11) P. Giannozzi et al., http://www.quantum-espresso.org.

(12) Mauri, F.; Pfrommer, B. G.; Louie, S. G. *Phys. Rev. Lett.* **1996**, *77*, 5300.

(13) Perdew, J. P.; Burke, K.; Ernzerhof, M. *Phys. Rev. Lett.* **1996**, *77*, 3865.

(14) Grossman, J. C.; Schwegler, E.; Draeger, E. W.; Gygi, F.; Galli, G. *J. Chem. Phys.* **2004**, *120*, 300.

(15) Schwegler, E.; Grossman, J. C.; Gygi, F.; Galli, G. *J. Chem. Phys.* **2004**, *121*, 5400.

(16) Pfrommer, B. G.; Mauri, F.; Louie, S. G. *J. Am. Chem. Soc.* **2000**, *122*, 123.

(17) Sprik, M.; Hutter, J.; Parrinello, M. *J. Chem. Phys.* **1996**, *105*, 1142.

(18) Sebastiani, D.; Parrinello, M. *Chem. Phys. Chem.* **2002**, *3*, 675.

(19) Modig, K.; Halle, B. *J. Am. Chem. Soc.* **2002**, *124*, 12031.

(20) Silvestrelli, P. L.; Bernasconi, M.; Parrinello, M. *Chem. Phys. Lett.* **1997**, *277*, 478.

(21) Ditchfield, R. *J. Chem. Phys.* **1976**, *65*, 3123.

(22) Modig, K.; Pfrommer, B. G.; Halle, B. *Phys. Rev. Lett.* **2003**, *90*, 075502.

(23) Zurek, E.; Pickard, C. J.; Walczak, B.; Autschbach, J. *J. Phys. Chem. A* **2006**, *110*, 11995.

(24) Sebastiani, D. *Chem. Phys. Chem.* **2006**, *7*, 164.

(25) Marques, M. A. L.; d'Avezac, M.; Mauri, F. *Phys. Rev. B* **2006**, *73*, 125433.

(26) Sebastiani, D.; Kudin, K. N. *ACS Nano* **2008**, *2*, 661.

(27) Besley, N. A.; Noble, A. *J. Chem. Phys.* **2008**, *128*, 101102.

(28) Stone, A. J.; Wales, D. J. *Chem. Phys. Lett.* **1986**, *128*, 501.

(29) Wang, H.-J.; Xi, X.-K.; Kleinhammes, A.; Wu, Y. *Science* **2008**, *322*, 80.